Check for updates

# A bioinspired Janus polyurethane membrane for potential periodontal tissue regeneration†

Yushui He,[a] Xiao Wang,[a] Yuanyuan He,[a] Xin Zhao,[a] Jingjing Lin,[a] Yuan Feng,[a] Jie Chen,[b] Feng Luo, [ID] *[a] Zhen Li,[a] Jiehua Li[a] and Hong Tan [ID] *[a]

Guided tissue regeneration (GTR) is the main therapeutic method for periodontal tissue regeneration. The key to the GTR strategy is the membrane which can assist the reconstruction of bone tissue in the periodontal defect and prevent the migration of epithelium and fibroblasts to the defect. However, the existing periodontal membrane cannot effectively promote periodontal tissue regeneration due to the limited bioactivity and physicochemical function. Here, we developed a bioinspired degradable polyurethane membrane with Janus surface morphology by integrating bioactive dopamine (DA) and an antibacterial Gemini quaternary ammonium salt (QAS). The Janus surface of the membrane is fabricated through spontaneous microphase separation, resulting from the different migration of functional segments between the air-contact upper surface with enriched antibacterial QAS and the substrate-contact bottom with enriched bioactive DA. The smooth surface of the upper membrane used to face the soft tissues can reduce cell adhesion to suppress the migration of fibroblasts, while the rough surface with a topological micro-pit structure of the bottom side facing the bone has excellent function of autonomic mineralization and cell adhesion to promote bone tissue reconstruction. In addition, the membrane containing the antibacterial QAS shows excellent antibacterial effect on common oral pathogens, such as *S. aureus* and *S. mutans*. Moreover, the specific dopamine group also endows the membrane with excellent antioxidant efficiency. *In vivo* research shows that this Janus polyurethane membrane can effectively promote periodontal tissue regeneration in a rat periodontal defect model. Combined with its excellent mechanical properties and biocompatibility, the polyurethane membrane is a promising material for potential periodontal tissue regeneration.

## 1. Introduction

Periodontitis is one of the most common oral inflammatory diseases in the world, which is a type of chronic and destructive inflammation disease.[1,2] If left untreated or improperly treated, it can result in loss of periodontal attachment, progressive bone loss, tooth loosening, and eventually early tooth loss.[3,4] This will seriously affect people's chewing and facial beauty, causing great life and psychological distress to human beings. What's more, bacteria in the periodontal pocket may enter the circulatory system and infect nearby or distant tissues and organs.[2] Severe periodontitis is also associated with many systemic diseases such as diabetes and cardiovascular disease.[5] Therefore, how to effectively treat periodontitis is of vital significance for human health and quality of life.

Guided tissue regeneration (GTR) is a common method used in clinical treatment of periodontitis.[6,7] The principle of this approach is to use a membrane material as a physical barrier to block the migration of epithelial cells and fibrous connective tissue to the defect site, providing space and time for the reattachment of the periodontal ligament and cementum.[8] At present, the membrane materials that have achieved clinical application can be divided into two types: one is an absorbable membrane, and the other is a non-absorbable membrane.[9] The most widely used non-absorbable membrane is expanded

[a] *College of Polymer Science and Engineering, State Key Laboratory of Polymer Materials Engineering, Sichuan University, Chengdu 610065, China.*
*E-mail: fengluo@scu.edu.cn, hongtan@scu.edu.cn*
[b] *Department of Pediatric Dentistry, West China School of Stomatology, Sichuan University, Chengdu 610065, China*

† Electronic supplementary information (ESI) available: Synthesis scheme and ^{1}H NMR spectra of LDA and EG12. Schematic diagram of the synthetic route of polyurethane. The proportion of elements on the smooth surface of polyurethane membranes obtained from XPS. The proportion of elements on both sides of the PU-LE5 membrane obtained from XPS. Color change of deionized water after PU-LE1 membrane soaking in water. Morphology of the PU-LE1 membrane before and after soaking in water. Colony growth of *S. aureus* and *S. mutans* cultured in medium as a blank control. Qualitative and quantitative analysis of polyurethane membranes co-cultured with *E. coli*. The Ca/P ratio of the minerals on the surface of polyurethane membranes obtained from EDX. Macro morphology of polyurethane membranes soaked in SBF for one week. Live/dead staining images of L929 implanted on rough and smooth surfaces of polyurethane membranes for 3 days and quantitative analysis of cell adhesion. See DOI: 10.1039/d1tb02068d

**2602** | *J. Mater. Chem. B*, 2022, **10**, 2602–2616

This journal is © The Royal Society of Chemistry 2022

polytetrafluoroethylene (e-PTFE). Because of its excellent mechanical properties to maintain enough space for regeneration, it has achieved a good regeneration effect in clinical application.[10] Unfortunately, due to its non-biodegradable defects, a second surgical removal may lead to infection of the regenerated tissue.[6] Alternatively, absorbable membranes are more applicable because they degrade over time and do not require subsequent surgical removal. However, the absorbable membrane also has its own defects. For example, collagen membrane has the advantages of good biocompatibility and is conducive to cell adhesion, but its rapid degradation rate and poor wet mechanical properties limit its clinical application.[11,12] The synthetic degradable polylactic acid membrane has relatively excellent mechanical properties, but its acid degradation products can easily trigger an inflammatory reaction.[13] These periodontal membrane defects lead to unsatisfactory overall clinical outcomes of the GTR strategy for periodontal disease.[14,15] In addition, the oral environment is complex with a wide variety of bacteria, and the periodontal membrane as an implant material is vulnerable to bacterial infection.[16] However, both absorbable and non-absorbable membranes often only serve as physical barriers and lack appropriate antibacterial properties. In previous GTR strategies, systemic antibiotic treatment after periodontal implantation was usually required to avoid microbial infection, which often causes systemic toxicity and bacterial resistance to the human body.[17] Therefore, it is necessary to develop a multi-functional periodontal membrane to solve the dilemma of current GTR strategies.

Recently, a GTR membrane with an asymmetrical double-sided function, which showed a better regeneration effect, may be a promising choice.[18] This is because the GTR membrane is in a relatively complex microenvironment.[8] The outer side of the membrane is the gums and fibrous connective tissue, and the inner side is the defective periodontal tissue. This requires that the outer side of the membrane can prevent the invasion of soft tissues, such as containing the function or morphology to inhibit cell adhesion and migration, while the inner side needs to have the function of promoting the repair of damaged periodontal tissue, such as cell adhesion, osteogenesis, and anti-oxidation.[19] However, designing a GTR membrane with a rational asymmetric function for periodontal tissue regeneration is still a challenge. The abundant asymmetrical structures and functions in nature give us enlightening inspiration.[20–22] For example, there is a Janus microstructure in the operculum of river snails. The outside of the operculum is a concentric ring structure to lubricate and reduce drag, while the inner surface of the operculum with a continuous micro-pit structure strongly bonds with the tissue of the river snail.[21] This Janus microstructure with an asymmetric function provides enlightenment to design a bionic membrane with a Janus structure and function for GTR.

Polyurethane (PU), which has good biocompatibility, excellent mechanical properties, and flexible designability,[23] is a promising biomaterial for preparing an asymmetric functional membrane through a specific phase separation procedure.[24,25] In our previous report, a membrane with an antibacterial

upper-layer, antifouling sub-layer and hydrophobic bottom layer was prepared by simply casting waterborne polyurethanes with multifunctional blocks.[24] Also, a biomimetic hierarchical structure with a hydrophilic surface and a hydrophobic subsurface was constructed from waterborne polyurethanes containing a self-assembling peptide extender.[25] Considering the asymmetric functional requirements of GTR membranes for periodontal tissue regeneration, the well-designed functional segments should be contained in the PU to facilitate the formation of an asymmetric double-sided function. The segments of polyethylene glycol (PEG) in PU tend to form a hydrophilic layer to decrease cell adhesion,[26] while importing bioactive segments can promote cell adhesion and cell proliferation. Importing dopamine (DA) segments is a relatively simple and efficient method to enhance bioactivity,[27,28] because the mussel adhesion protein-inspired substance gives the material strong adhesion, as well as promoting cell adhesion. In addition, dopamine can also endow materials with excellent mineralization and antioxidant capacity, which are all favorable factors for periodontal tissue regeneration.[29,30] Besides chemical modification to introduce bioactive segments, physical modification is also an effective method to affect cell behaviors.[31] A special microscopic topology to mimic the extracellular matrix (ECM) is beneficial to the cell adhesion behavior from the 2D mode to 3D mode.[32] In addition, ridge, well, sphere, and honeycomb structures are verified to have the magical effects of regulating cell behavior and changing cell fate.[31,33] For example, Chen et al. constructed fluted structures on membrane surfaces that significantly promoted the adhesion of cancer cells and mesenchymal stem cells.[34] Furthermore, physical modification can also give the material an anisotropic surface with Janus morphology and function.[22]

To resist bacterial infection and ensure the smooth progress of periodontal tissue regeneration, high quality periodontal membranes should also have excellent antibacterial function.[35] However, current research on the antibacterial periodontal membrane is mostly limited to the use of traditional antibiotics and metal nanoparticles.[1,17,36] This will bring the risk of bacterial resistance and local heavy metal accumulation, which is unfavorable to periodontal regeneration.[2] Quaternary ammonium salts (QASs) are a kind of bactericide with a wide antibacterial spectrum, good stability, and high antibacterial activity and it is difficult for them to produce bacterial resistance.[37,38] They have been widely used in many commercial products such as circulating water microbicides, mouthwash and contact lens solutions.[39] The bactericidal mechanism of a QAS is the electrostatic interaction between its own positive charge and the negative charge on the bacterial cell membrane. When the bacteria approach, the hydrophobic alkyl chain will prick the bacterial cell membrane to make the intracellular substances of the bacteria flow out, leading to the death of the bacteria.[40,41] This unique bactericidal mechanism has advantages over antibiotics and metal nanoparticles. In addition, our research group has realized the introduction of a Gemini QAS into the polyurethane chain. In the process of forming the membrane, the quaternary ammonium salt group spontaneously transfers to the surface of the polyurethane membrane to form a sterilization layer, which makes
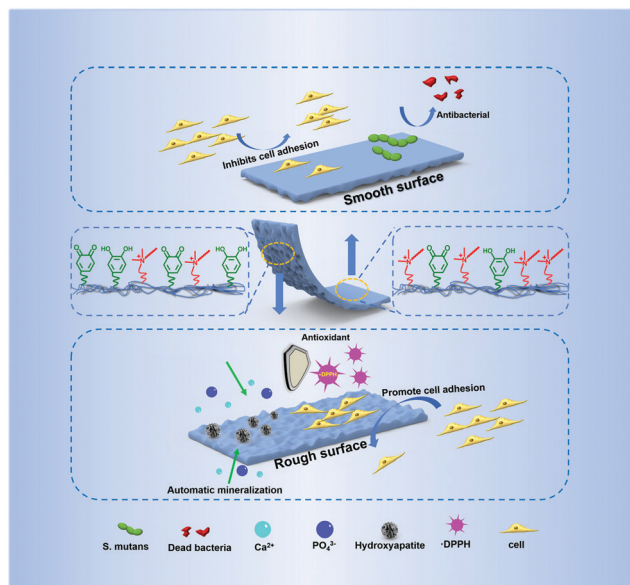
Fig. 1 Schematic of the morphology and function of Janus polyurethane periodontal membrane.

the polyurethane membrane have an excellent sterilization effect and durable antibacterial aging.[24,39]

In this work, inspired by the Janus character of the operculum of the river snail, we developed a kind of degradable polyurethane periodontal membrane with Janus function and morphology by integrating the bioactive DA and the antibacterial Gemini QAS (Fig. 1). The membrane possesses a smooth surface on the upper side and a topological micro-pit structure on the bottom side. The Janus surface of the membrane is fabricated through a spontaneous microphase separation, resulting from the different migration of functional segments between the air-contact upper surface with enriched antibacterial QAS and the substrate-contact bottom with enriched bioactive DA. We demonstrated that such anisotropic morphology produces a different cell fate on the respective surface, and the introduction of quaternary ammonium salts and the dopamine group can endow the membrane with multiple functions including antibacterial properties, antioxidant properties, and autonomic mineralization properties. In addition to *in vitro* experiments, we also verified the promoting effect of this Janus polyurethane membrane on periodontal tissue regeneration in a rat periodontal defect model.

# 2. Materials and methods

## 2.1. Materials

Polyethylene glycol (PEG, molecular weight 1450, Dow Chemical) and polycaprolactone (PCL, molecular weight 2000, Dow Chemical) were dehydrated under vacuum at 95 °C for 2 hours before use. L-Lysine diisocyanate (LDI, Nantong Dahong Chemical Industry Limited Company) was redistilled under vacuum before use. 1,4-Butanediol (BDO), *N,N*-dimethylformamide (DMF) and triethylamine (TEA) were purchased from Chengdu Kelong Reagent Co. 1-Bromododecane and 1,3-propane diamine were obtained from Shanghai Aladdin Reagent Co. 3-Hydroxytyramine hydrochloride was purchased from Adamus Reagents Co. (S)-2,6-Bis-*tert*-butoxycarbonylaminohexanoic acid was supplied by Sichuan Ampebiochem Co. Organic bismuth (The Shepherd Chemical Company) was used as the catalyst. Brain heart infusion broth (BHI) was provided by Shandong Tuopu Biol-engineering Co. Artificial saliva and simulated body fluid (SBF) were received by Beijing Solarbio Science & Technology Co. 1,1-Diphenyl-2-trinitrophenylhydrazine (DPPH) was purchased from Tixie Chemical Industrial Development Co.

## 2.2. Synthesis of polyurethane

The lysine-derivative Gemini quaternary ammonium salt (EG12) and lysine-dopamine (LDA) as the chain extenders were synthesized in our laboratory according to our previous method.[39,42] Then the polyurethane was synthesized using PEG, PCL, LDI, BDO, EG12 and LDA. The synthetic procedure of polyurethane is as follows. First, PEG and PCL were added into a three-necked flask and dehydrated under vacuum at 95 °C for 2 hours. When the temperature of the mixture was reduced to 60 °C, LDI and 0.1% organic bismuth were added. This reaction continued for 2 hours at 80 °C. Then, after the prepolymer temperature was lowered to 65 °C, BDO was added and reacted for 2 hours at 75 °C. Finally, EG12 and LDA were added and reacted for 3 hours at room temperature. The composition and the molecular weight of polyurethane are shown in Table 1. The specimens were denoted as PU-BDO, PU-BE, PU-BL, PU-LE1, PU-LE3 and PU-LE5, where B, L and E stand for BDO, LDA and EG12, respectively. The number represents the proportion of EG12 to chain extender.

## 2.3. Preparation of the polyurethane membrane

First, the polyurethane was precipitated with water and redissolved in DMF. Then, it was poured into a siliconized glass dish. After drying in a blast oven at 50 °C for 4 days, a certain

Table 1 Theoretical composition and the molecular weight of the PU samples

| Sample | Mole ratio | | | NCO/(OH + NH$_2$) | M(LDA)/M (all) (%) | M(EG12)/M (all) (%) | $M_n$ (g mol$^{-1}$) |
|---|---|---|---|---|---|---|---|
| | PEG : PCL | LDI | LDA : BDO : EG12 | | | | |
| PU-BDO | 5:5 | 20.4 | 0:10:0 | 1.02 | — | — | 73 213 |
| PU-BE | 5:5 | 20.4 | 0:5:5 | 1.02 | — | 16.55 | 30 315 |
| PU-BL | 5:5 | 20.4 | 5:5:0 | 1.02 | 5.93 | — | 31 426 |
| PU-LE1 | 5:5 | 20.4 | 5:4:1 | 1.02 | 5.74 | 3.61 | 27 695 |
| PU-LE3 | 5:5 | 20.4 | 5:2:3 | 1.02 | 5.39 | 10.17 | 24 808 |
| PU-LE5 | 5:5 | 20.4 | 5:0:5 | 1.02 | 5.08 | 15.98 | 21 655 |

**2604** | *J. Mater. Chem. B*, 2022, **10**, 2602–2616

This journal is © The Royal Society of Chemistry 2022

amount of water was added to the glass dish to swell the polyurethane membrane and separate it from the glass dish. The polyurethane membrane was removed and soaked in deionized water for 3 days to remove small molecules, and then dried again.

## 2.4. Characterization

**2.4.1. Fourier transform infrared (FTIR) spectra.** The Fourier transform infrared (FTIR) spectra analysis of polyurethane membranes was carried out using a Nicolet iS50 infrared spectrometer in the attenuated reflectance mode (ATR). The spectra measurement range was 4000–400 cm$^{-1}$ with 32 scans per measurement and a resolution of 4 cm$^{-1}$.

**2.4.2. $^1$H-NMR spectra.** $^1$H NMR spectra were obtained using a Bruker 400 MHz NMR spectrometer at room temperature. The samples were dissolved in deuterated dimethyl sulfoxide (DMSO).

**2.4.3. Gel permeation chromatography (GPC).** The number average molecular weight ($M_n$) of polyurethane was determined by GPC. 2 g lithium bromide dissolved in 1 L DMF was used as the mobile phase and PMMA was used as the standard sample. The flow rate was 1.0 mL min$^{-1}$ at 40 °C. All samples were filtered by a 0.22 μm hydrophobic membrane when injected with GPC.

**2.4.4. Water absorption performance.** The water absorption property of polyurethane membranes was tested ($n = 3$). Briefly, the dried polyurethane membranes were cut into a wafer with a diameter of 1 cm and weighed to get the initial weight ($W_i$). Then, the wafers were immersed in artificial saliva at 37 °C for 48 h to obtain the swelling equilibrium weight ($W_e$). The saliva uptake ($W_s$) of the samples was calculated as follows:

$$W_s(\%) = \frac{W_e - W_i}{W_e} \times 100\%$$

**2.4.5. Water contact angle test.** The surface hydrophilicity of polyurethane membranes was measured using a digital optical contact angle tester (DSA-100, KRUSS GmbH) at room temperature ($n = 5$). During the measurement, a 2 μL deionized water droplet was dropped on the surface of polyurethane membranes and the angle of both sides was measured.

**2.4.6. Scanning electron microscope (SEM).** The morphology of both sides of the polyurethane membranes was investigated using SEM (Nova Nano SEM450, 5kV). All samples were sprayed with gold before testing.

**2.4.7. X-ray photoelectron spectroscopy (XPS).** The surface element analysis of polyurethane membranes was determined by X-ray photoelectron spectroscopy (XSAM-800X). The X-source is an Al Kα ray gun (20 kV, 10 mA) with a take-off angle of 90°.

**2.4.8. *In vitro* degradation test.** The *in vitro* degradation behavior of the polyurethane membranes was tested using artificial saliva ($n = 3$). The samples were weighed to obtain their initial weight ($W_o$) and placed into a centrifuge tube containing 5 mL artificial saliva. Then, the centrifuge tubes were placed in a constant temperature water bath shaker with a temperature of 37 °C and a rotation rate of 90 rpm. The degradation of the samples in 60 days was observed under the condition of weekly replacement of artificial saliva. At a predetermined time, the samples were obtained and rinsed with deionized water three times, then freeze-dried to a constant weight ($W_t$). The weight loss was determined as follows:

$$\text{weight loss } (\%) = \left(1 - \frac{W_t}{W_o}\right) \times 100\%$$

**2.4.9. Oxidation resistance.** A DPPH free radical elimination method was used to evaluate the antioxidant properties of polyurethane membranes ($n = 3$).[43] First, 0.2 mM DPPH solution was prepared with ethanol as the solvent under the condition of avoiding light. Then 0.1 g of the shredded polyurethane membranes were weighed and placed in a centrifuge tube containing 2 mL DPPH solution. The O.D. value of the DPPH solution ($A_s$) at 517 nm was detected using an ultraviolet spectrophotometer (Shanghai Meipuda, UV-1800) after reaction for 1 h at room temperature in dark conditions. The O.D. value of the DPPH solution without samples ($A_{ctr}$) was used as the blank control. The DPPH free radical scavenging rate of the samples was calculated according to the following formula:

$$\text{DPPH scavenging } (\%) = \left(1 - \frac{A_s}{A_{ctr}}\right) \times 100\%$$

**2.4.10. Mineralization ability of the membrane.** The mineralization ability of polyurethane membranes was evaluated *in vitro* according to the literature.[44] Briefly, the samples were incubated in a centrifuge tube containing 10 mL of simulated body fluid at 37 °C and the simulated body fluids were changed daily. After 7 days, the samples were washed with deionized water 3 times and freeze-dried. The surface morphology and elemental composition of the polyurethane membranes were studied using SEM and an energy dispersive x-ray spectrometer (EDX).

**2.4.11. Mechanical performance test.** The mechanical properties of wet polyurethane membranes were evaluated using a uniaxial tensile method on a universal testing machine (Dongguan lixian instrument Scientific Co. Ltd, HZ-1004, China) at 25 °C. The dumbbell type samples were stretched at a speed of 300 mm min$^{-1}$ to obtain the typical stress–strain curve ($n = 5$). Then, the ultimate tensile strength, ultimate strain and Young's modulus were obtained from the stress–strain curves.

**2.4.12. *In vitro* antibacterial evaluation.** *Staphylococcus aureus* (*S. aureus*, ATCC 25923) and *Streptococcus mutans* (*S. mutans*, ATCC 35668) were selected to evaluate the antibacterial properties of polyurethane membranes *in vitro*. Briefly, bacteria were inoculated in BHI medium at 37 °C overnight and then the bacterial solution was diluted to a concentration of 10$^6$ CFU mL$^{-1}$. Next, a circular polyurethane membrane with a diameter of 1 cm was placed in a 48-well plate and 300 μL of bacterial solution was added to the membrane for co-culture at 37 °C for 24 h ($n = 3$). At a predetermined time, the bacterial liquid was diluted with the culture medium and coated on the agar (Solarbio, Beijing) plate. 24 h later, the number of colonies was counted ($n = 3$). The untreated bacterial liquid was used as the blank control.

This journal is © The Royal Society of Chemistry 2022

*J. Mater. Chem. B*, 2022, **10**, 2602–2616 | **2605**

## 2.5. Cell experiment

**2.5.1. Cell culture.** Mouse fibroblasts (L929) and rat bone marrow mesenchymal stem cells (rBMSCs) were provided by the Laboratory of Internal Medicine, West China Hospital, Sichuan University, China. L929 cells were cultured in Dulbecco's modified Eagle's medium (DMEM, Thermo Fisher, Beijing) supplemented with 10% fetal bovine serum (FBS, Thermo Fisher, Beijing) and 1% penicillin/streptomycin (Solarbio, Beijing). Different from L929, rBMCs were cultured in DMEM/low glucose (Thermo Fisher, Beijing). All cells were cultured in 5% carbon dioxide and about 90% relative humidity.

**2.5.2. Cytotoxicity test of polyurethane membranes.** The cytotoxicity of polyurethane membranes was tested using a Methyl Thiazolyl Tetrazolium (MTT, Millipore Sigma Canada Co) assay. First, the extraction solution was prepared by immersing 0.1 g polyurethane membrane in 1 mL complete culture medium for 24 h. Then the extract was diluted by a factor of 10, 100, and 1000 and was added to a 96-well plate containing $10^4$ cells per well. MTT was added after a day of culture at 37 °C, and the O.D. value of the experimental group at 490 nm was measured with a microplate reader (DNM-9602, PERLONG, China). The O.D. value of the complete medium well was used as the blank control. Cell viability was obtained using the following formula:

$$\text{Cell viability (\%)} = \frac{\text{O.D.}_{\text{sample}}}{\text{O.D.}_{\text{control}}} \times 100\%$$

**2.5.3. Cell adhesion test on both sides of the polyurethane membranes.** The adhesion property of cells to the polyurethane membranes was tested by the method of standard live/dead staining assay (Calcein-AM/PI Double Stain Kit, Solarbio, Beijing). Briefly, the polyurethane membrane was cut into 1 cm diameter wafers and divided into two groups: smooth (upper) surface and rough (bottom) surface. Then, the two groups of membranes were placed in a 48-well plate and soaked overnight with phosphate buffer saline (PBS, Thermo Fisher, Beijing). Next, PBS was sucked out during the experiment and $10^5$ cells were added to each well. After three days of culture, the culture medium was sucked out and washed twice with PBS to remove the unadhered cells. Finally, 400 μL of staining solution (4 μM Calcein-AM Solution and 6 μM PI Solution) was added to the wells and incubated at 37 °C for 20 min. The cell adhesion area was analyzed using a laser scanning confocal microscope (Nikon N-SIM) and quantified using Image J software.

**2.6. *In vivo* biological evaluation.** According to previous literature, the periodontal tissue regeneration ability of the Janus polyurethane membrane was evaluated using a rat periodontal defect model *in vivo*.[2] All animal experiments were approved by the ethics committee of Sichuan University. Eight-week-old female Sprague-Dawley rats (200–250 g) were purchased from the Animal Center of Sichuan University (Sichuan, China) for the *in vivo* experiments. Briefly, the rats were anesthetized and the gingival flap was opened with a scalpel. Then, the periosteal separator was used to expose the alveolar bone of the maxillary first molar. Part of the alveolar

bone of the first molar was removed (length: 3 mm; width: 1 mm; depth: 2 mm) with a drill under continuous saline irrigation. Finally, a polyurethane membrane was placed on the periodontal defect and the wound was sutured. A total of 16 SD rats were randomly divided into 4 groups (*n* = 4 per group): (i) the normal group, (ii) the periodontal defect group without a polyurethane membrane (control), (iii) the PU-BDO group, and (iiii) the PU-LE5 group. Four weeks later, the animals were sacrificed and the defective maxilla was collected. A microcomputed tomography (micro-CT) instrument (Quantum GX II, PerkinElmer) was used to analyze the amounts of recovered bone at the defect sites.

## 2.7. Statistical analysis

The values were expressed as mean ± standard deviation (SD) and at least an average of three parallel experiments. A statistical difference was considered when $p < 0.05$ by one-way analysis of variance: $*p < 0.05$, $**p < 0.01$, $***p < 0.001$.

# 3. Results and discussion

## 3.1. Synthesis and characterization of polyurethane membranes

LDA and EG12 as chain extenders were first synthesized (Fig. S1 and S2, ESI†), and then successfully combined into the polyurethane (Fig. 2a). The synthesis route of polyurethane is shown in Fig. S3 (ESI†). As listed in Table 1, the molecular weight of polyurethane decreased with the introduction of EG12 and LDA, which may be due to the large polarity and steric hindrance of the two chain extenders. In order to prove the polyurethanes, FTIR was used to characterize its chemical structure (Fig. 2b). The typical characteristic peaks of polyurethane are reflected in the spectrum. The peaks at 3500 cm$^{-1}$–3330 cm$^{-1}$ correspond to the tensile vibration of N–H, the peaks at 2934 cm$^{-1}$ – 2870 cm$^{-1}$ correspond to the stretching vibration of C–H, and the C=O stretching vibration near 1728 cm$^{-1}$ and the C–O–C stretching vibration near 1100 cm$^{-1}$ can also be found in the FTIR. In addition, the stretching vibration region of C–N and the deformation vibration region of N–H appeared near 1540 cm$^{-1}$, which proved the formation of a carbamate bond.

In addition, the structure of the polyurethane was further characterized through $^1$H NMR spectra (Fig. 2c and 2d). The chemical shifts at 3.98 (–CO–O–C$\underline{H}_2$–), 2.27 (–O–CO–C$\underline{H}_2$–), 1.54 (–O–CH$_2$–C$\underline{H}_2$-) and 1.29 (-CH$_2$–C$\underline{H}_2$–CH$_2$-) ppm corresponded to the methylene proton on the PCL. The chemical shifts at 3.08 (–N$^+$(C$\underline{H}_3$)$_2$–) and 0.85 (–CH$_2$–C$\underline{H}_3$) are assigned to the H protons of the methyl on the N$^+$ element and the methyl at the end of the alkyl chain in the chain extender EG12. The chemical shifts at 6.42–6.61 ppm and 8.67 ppm corresponded to the H protons of the benzene ring and the phenolic hydroxyl group in LDA. The chemical shifts of the H proton on PEG, BDO and LDI can also be found in the $^1$H NMR spectra, which are marked in Fig. 2a. The above results prove the successful synthesis of polyurethane.
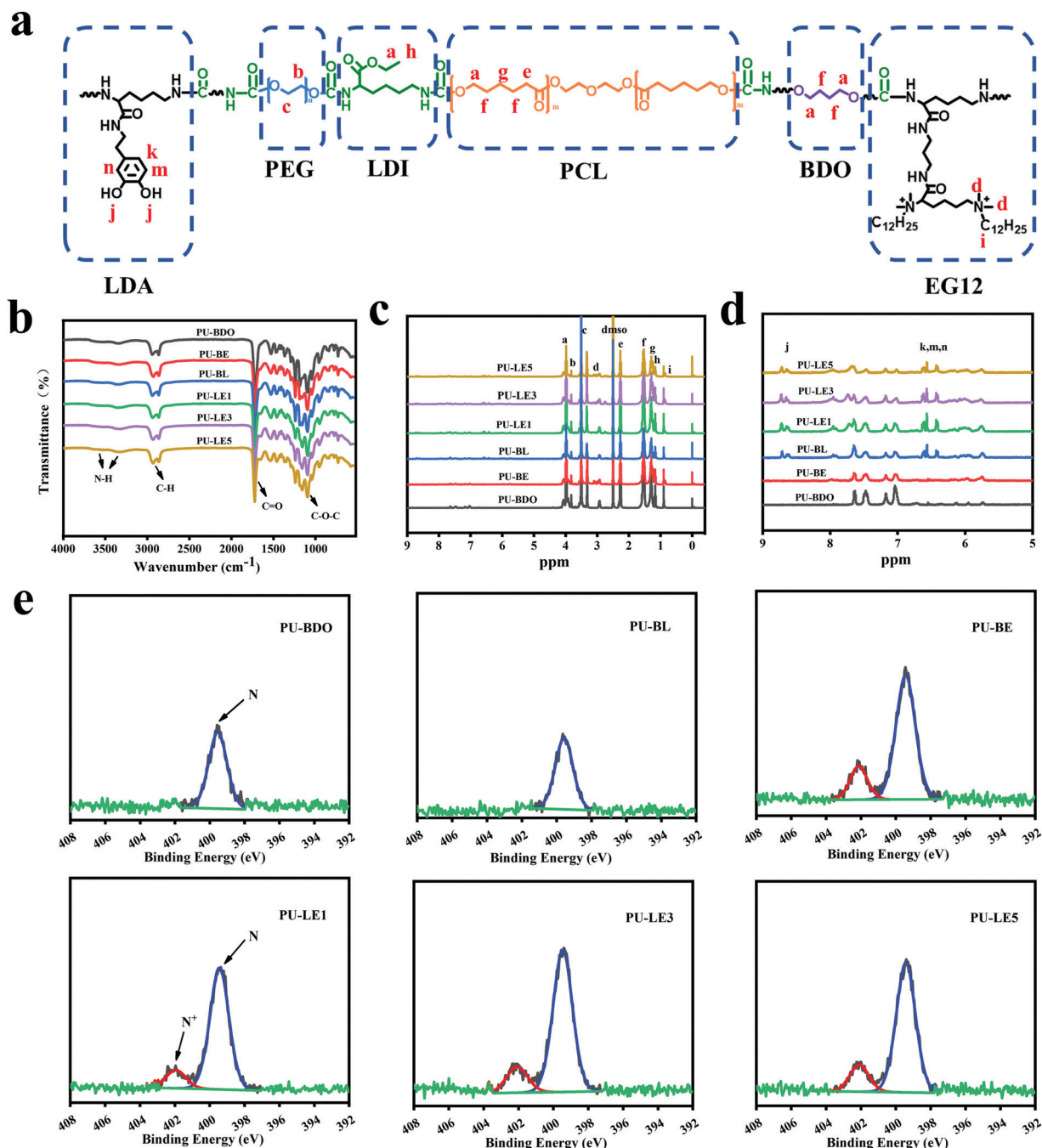
Fig. 2 (a) Structural formula of the representative polyurethane. (b) FTIR spectra of polyurethane membranes. (c) ^{1}H NMR spectra of polyurethane membranes. (d) Magnified ^{1}H NMR spectra from 5 to 9 ppm. (e) N 1s XPS spectra of polyurethane membranes.

The content of $N^+$ element on the surface has a significant effect on the antibacterial effect,[45,46] which is of inestimable importance to the polyurethane membranes. Thus, the content of $N^+$ element on the smooth surface of polyurethane membranes was analyzed by XPS. As shown in Fig. 2e, except for PU-BDO and PU-BL, an additional characteristic peak of $N^+$ element appeared near 402 eV in all the other samples, and with the increase of EG12 content, the proportion of $N^+$ element in N 1s also increases (Table S1, ESI†). This indicates that polyurethane membranes with different quaternary ammonium

salt content on the surface were prepared. Notably, the actual $N^+$ element content on the surface of the polyurethane membrane is higher than the theoretical value, which may be due to the high surface activity and interfacial energy of the QAS, leading to the migration of EG12 to the surface during the membrane forming process.[24,47]

Since the LDA and EG12 possess different spatial structure and interfacial energy,[47–49] it is expected that distinguishing the phase separation of the polyurethane membranes will depend on the content of these two extenders. Particularly, for the
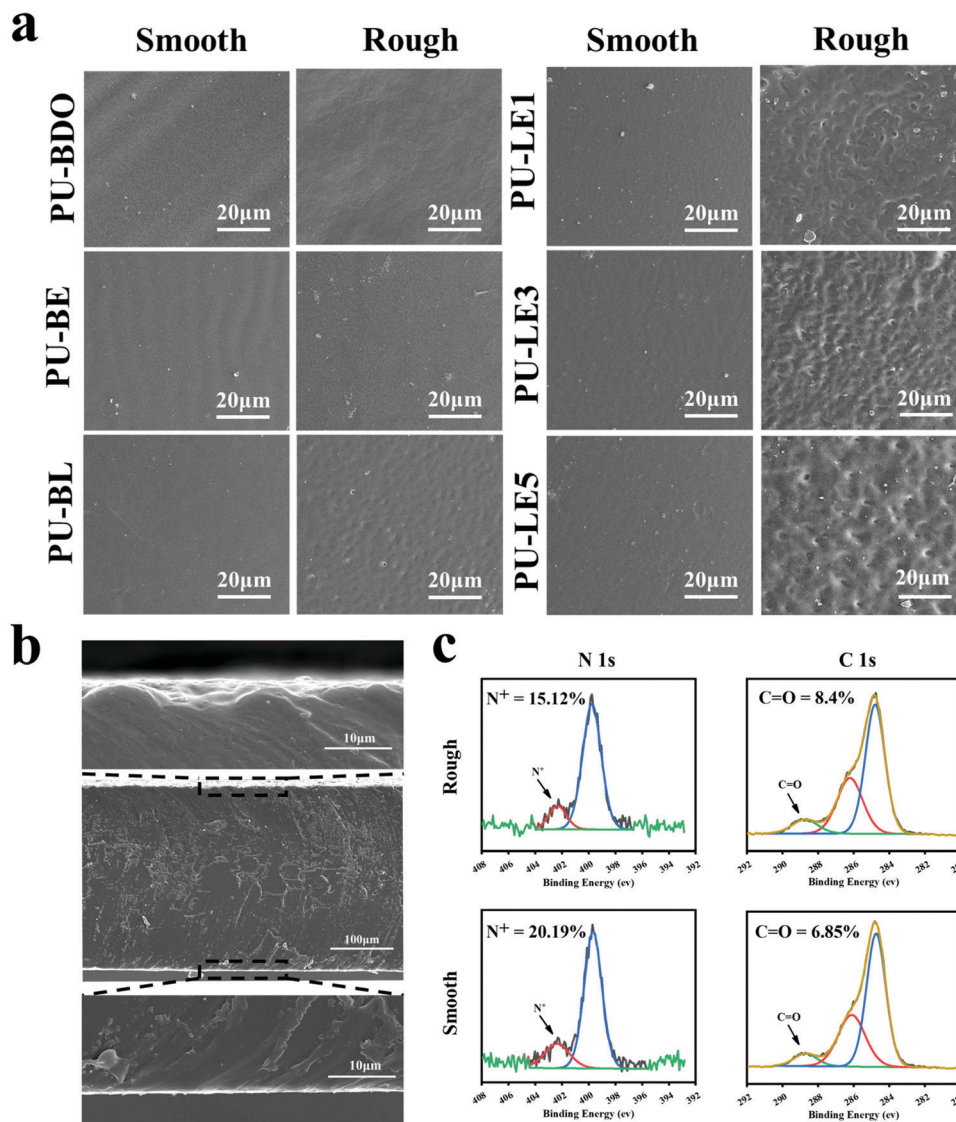
This journal is © The Royal Society of Chemistry 2022

J. Mater. Chem. B, 2022, 10, 2602–2616 | 2607

**Fig. 3** (a) Morphology of both sides of the polyurethane membranes. (b) Section morphology of the PU-LE5 membrane. The enlarged pictures show the rough substrate–contact surface (up) and the smooth air-contact surface (down). (c) N 1s and C 1s XPS spectra of the PU-LE5 membrane.

polyurethane membranes with an added LDA extender, the two sides of the membranes are completely different, which are smooth on the upper air-contact side and rough with a micro-pit on the bottom substrate-contact side, as shown in Fig. 3a. Moreover, the micro-pit is only in a scale of several microns in depth (Fig. 3b), indicating that spontaneous microphase separation occurs at the interface in contact with the siliconized glass dish because of importing LDA. This asymmetrical morphology is much like the Janus character of the operculum of river snails. In contrast, the two sides of the polyurethane membranes without an LDA chain extender have a similar morphology to the smooth surface. In order to explore the reason for forming this Janus morphology, surface elements on both sides of the PU-LE5 membrane were further analyzed by XPS (Fig. 3c and Table S2, ESI†). It was found that the $N^+$ content on the smooth surface of the polyurethane membrane (20.19%) was much more than that on the rough surface (15.12%), while the C=O content was lower.

These results indicated that the smooth surface had more quaternary ammonium salt groups and the rough surface had more dopamine groups (phenol hydroxyl oxidizes to quinone[42]). This spontaneous microphase separation depends on the different migration of functional segments between the Gemini QAS and LDA. That is, the positively charged Gemini QAS can accumulate at membrane/air interfaces owing to its high interfacial energy.[47] Meanwhile, the dopamine molecules tend to precipitate at the membrane/substrate interfaces owing to the catechol structure which can form multiple bond interactions with the siliconized glass dish.[50]

Regarding the micro-pit morphology, a possible explanation is that the LDA chain extender contains a benzene ring structure with a large steric hindrance, which leads to large phase separation from the hard segments of polyurethane and even then a small amount of LDA does not participate in the chain extension reaction.[51,52] During the process of forming the

**2608** | *J. Mater. Chem. B*, 2022, **10**, 2602–2616

This journal is © The Royal Society of Chemistry 2022

membrane, the quaternary ammonium salt group migrates to the upper surface of the polyurethane membrane, while the unreacted LDA molecules and enriched dopamine segments are repelled to the bottom substrate–contact surface.[24,25] When immersed in water, the unreacted LDA molecules and soluble dopamine segments dissolve out from the bottom side. Compared with the samples before immersing in water, the color change of deionized water from transparent to light brown, and the morphology change of the bottom substrate–contact surface of the PU-LE1 membrane from smooth to rough after immersing in water, can preliminarily demonstrate our conjecture (Fig. S4, ESI†). In summary, PU-LE series polyurethane membranes with different morphologies on both sides were fabricated, thus it arouses our interest to investigate the functional difference between the two sides.

Because the polyurethane membranes contain a degradable PCL soft segment, the hydrophilicity may affect the degradation behaviors,[26] so the hydrophilicity of the polyurethane membranes was first studied. As shown in Fig. 4a and b, the area of all samples did not change significantly before and after equilibrium swelling by artificial saliva and the water contents

of all membranes are between 35% and 42%. Moreover, compared with the PU-BDO sample, the water content of the membranes decreased slightly after the LDA chain extender was introduced, while the water content of polyurethane increased after EG12 was introduced. This may be caused by the distinguishing interaction in polyurethane for the two kinds of chain extender.[48] When LDA is introduced, due to the formation of a urea-group, more hydrogen bonds will be generated between the polyurethane molecular chains, so that the intermolecular force will be stronger, making it difficult for water molecules to enter. Although the introduction of EG12 will also increase the intermolecular force, the larger side groups of the positively charged EG12 will increase the hydrophilicity and enlarge the distance of the molecular chain, which is conducive to the entry of water molecules. Therefore, the final water content increases. As shown in Fig. 4c, the introduction of EG12 could significantly reduce the water contact angle of polyurethane membranes. The higher the content of EG12, the smaller the water contact angle. This is mainly due to the migration of quaternary ammonium salts to the surface of polyurethane membranes, which leads to the surface becoming
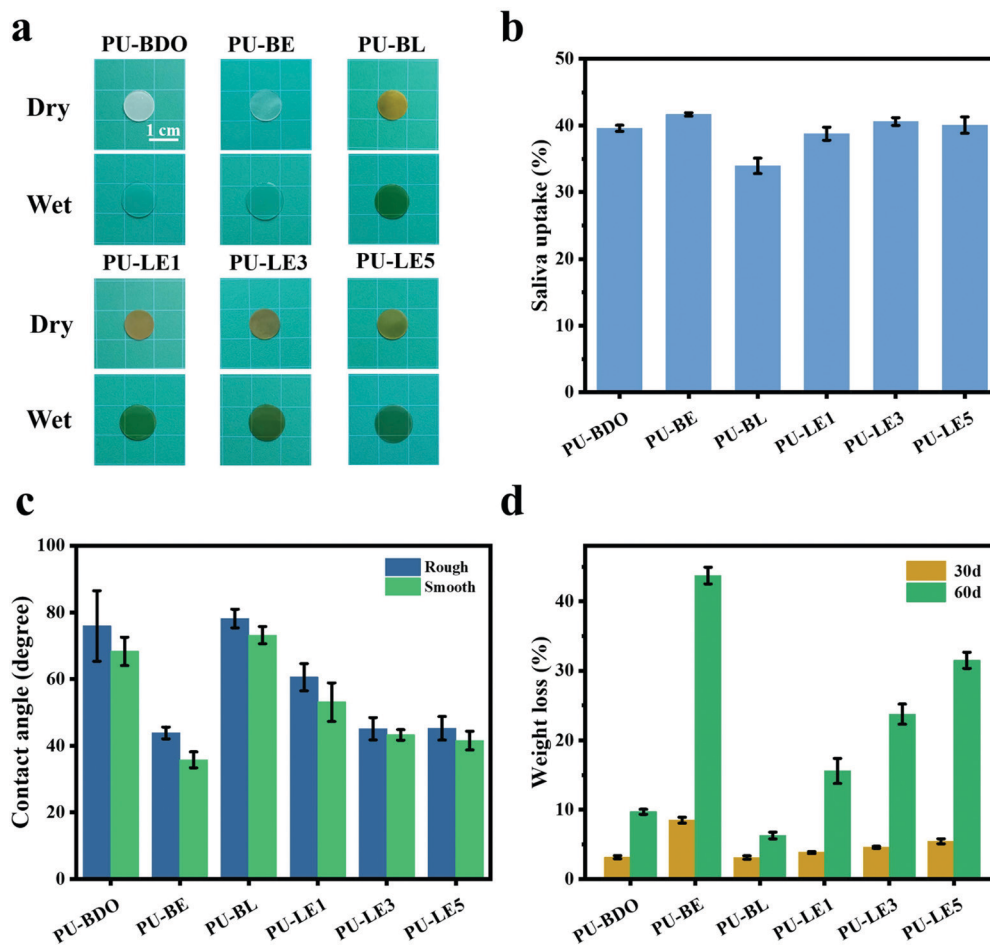


**Fig. 4** (a) Area comparison of polyurethane membranes before (Dry) and after (Wet) equilibrium swelling by artificial saliva. (b) The water content of the membranes after equilibrium swelling by artificial saliva. (c) Water contact angle of polyurethane membranes for smooth and rough surfaces. (d) Degradation behavior of the polyurethane membrane in artificial saliva for 2 months.

more hydrophilic.[24] According to the Wenzel equation, for a hydrophobic surface the increase of surface roughness can increase the water contact angle; for a hydrophilic surface, the water contact angle decreases with the increase of surface roughness.[53] Studies have found that the water contact angle of both smooth and rough surfaces is less than 90°, which are hydrophilic surfaces. Because of the micro-pit structure of the rough surface, its roughness is greater than the smooth surface. According to the Wenzel equation, the water contact angle of the rough surface should be lower than the smooth surface. But our results show that the rough surface actually has a higher water contact angle. It may be that the smooth surfaces with high hydrophilic GQA content are more conducive to the spread of water droplets than the rough surfaces.[54]

The degradation of polyurethane membranes corresponds to the hydrophilicity of polyurethane membranes. That is, the degradation rate of the PU-BE group was the fastest with the highest hydrophilicity, while the degradation rate of the poor hydrophilicity of the PU-BL group was the slowest (Fig. 4d). This is because the better the hydrophilicity, the more opportunities for the water molecules to make contact with the ester bond to accelerate the hydrolysis. On the other hand, the PU-LE5 membrane still has 68% of its initial mass after degradation in artificial saliva for two months, which can provide sufficient time for periodontal tissue regeneration.

## 3.2. Mechanical properties

The periodontal tissue regeneration membrane needs excellent mechanical properties to maintain the space under the membrane during the service period, and avoid the membrane damage caused by chewing food and other reasons to lose its effect.[3,55] The mechanical properties of polyurethane membranes were evaluated using a uniaxial tensile method. Fig. 5a is the typical stress–strain curves of wet polyurethane membranes. Fig. 5b–d corresponds to the ultimate tensile strength, ultimate strain, and Young's modulus, respectively. It was found that compared with the PU-BDO membrane (stress 4.73 MPa, strain 1708%), the mechanical properties of the PU-BE membrane were improved after the introduction of EG12, reflecting in the simultaneous improvement of the breaking strength (8.06 MPa) and elongation at break (1928%). This is because the generated urea group will form stronger hydrogen bonds, which increases the intermolecular force and improves the mechanical properties. Meanwhile, the introduction of LDA for PU-BL also increases the breaking strength (10.66 MPa), but reduces the elongation at break (1235%). The main reason is that the benzene ring structure of LDA will increase the rigidity of the molecular chain, which makes it difficult for the molecular chain to move, thus resulting in the reduction of the elongation at break. In addition, the ultimate tensile strength and ultimate strain decreased (Fig. 5b and c) with the increase of EG12 content, mainly because EG12 contains large side groups, which will reduce the formation
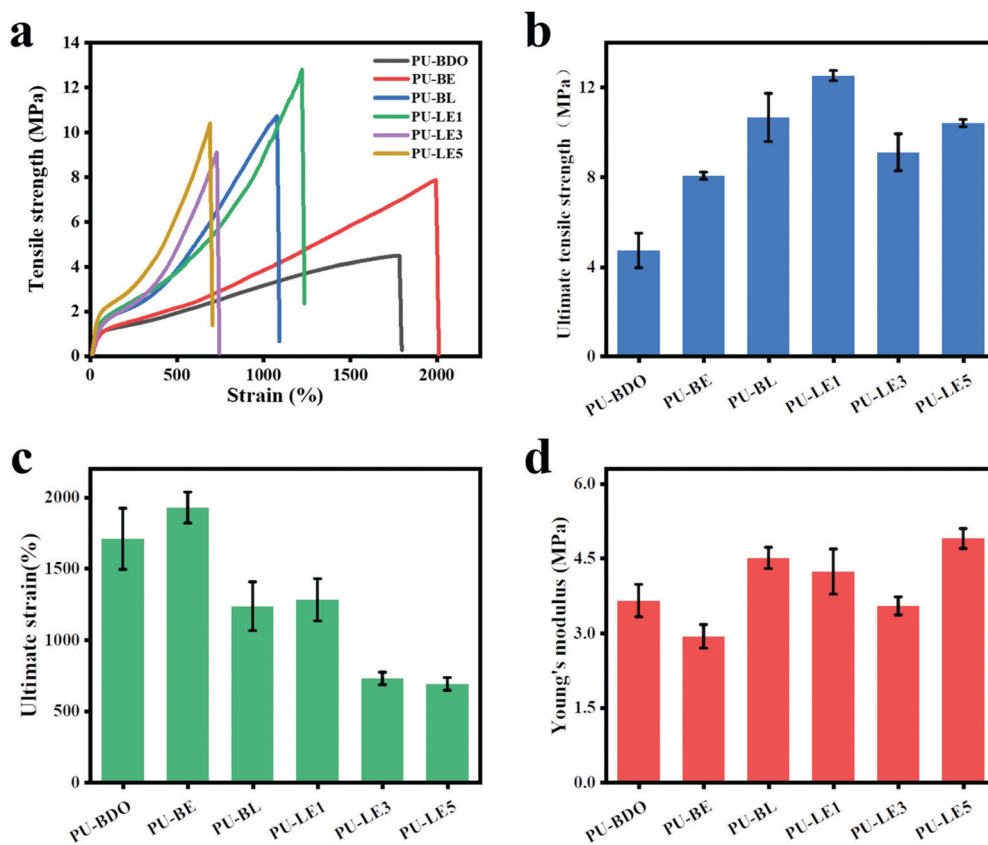


Fig. 5 (a) Stress–strain curves of polyurethane membranes. (b) Ultimate tensile strength. (c) Ultimate strain. (d) Young's modulus.

2610 | J. Mater. Chem. B, 2022, 10, 2602–2616

This journal is © The Royal Society of Chemistry 2022

of hydrogen bonds and make it more difficult to move the molecular chains. What's more, the low molecular weight of the series of PU-LE (Table 1) would also lead to a low elongation at break. As for the Young's modulus (Fig. 5d), the introduction of LDA improves the Young's modulus of the polyurethane membranes, but the introduction of EG12 reduces the Young's modulus, which is related to the hydrophilic feature of the EG12 compared with the hydrophobic benzene ring structure of LDA. Overall, the series of PU-LE membranes have excellent mechanical properties, which are better than most of the reported natural materials[44,56,57] and synthetic materials[2,7,58] used for periodontal tissue regeneration membranes.

### 3.3. Antibacterial properties

Due to the complex oral microenvironment, the periodontal regeneration membrane as an implant material is inevitably faced with the risk of bacterial infection, and periodontal tissue is also threatened by bacterial infection during the process of regeneration.[2,6] Therefore, *S. aureus* (a typical Gram-positive bacteria) and *S. mutans* (one of the most plentiful bacteria in oral biofilm[59]) were chosen to explore the antibacterial

properties of polyurethane membranes. The diluting bacterial solutions which are cultured with the polyurethane membranes are shown in Fig. 6a, b and Fig. S5 (ESI†). Apparently, the antibacterial effect enhances with increasing EG12 content of the samples. Except for PU-LE1, the PU-LE series of polyurethane membranes have excellent antibacterial efficiency above 90% on both *S. aureus* and *S. mutans*. In contrast, the samples of PU-BDO and PU-BL without EG12 show a relatively weak antibacterial effect. This is because EG12 contains a positively charged quaternary ammonium salt group that attracts the bacteria with a negative surface charge, and the long hydrophobic alkyl chain will pierce the bacterial cell membrane, causing the intracellular material to flow out and eventually kill the bacteria.[38] The weak antibacterial effect of PU-BDO and PU-BL may be due to the adsorption of nutrients in the medium by polyurethane, which affects bacterial proliferation. As shown in Fig. 6c and d, the antibacterial effect was related to the amount of EG12, and the more EG12 introduced, the better the antibacterial effect. This is also consistent with the increasing GQA content in the surface of the membrane as verified by the XPS results. In addition, SEM was used to observe the



**Fig. 6** Colony growth of *S. aureus* (a) and *S. mutans* (b) cultured with polyurethane membranes at different dilutions. The numbers 1–8 represent the samples diluted $10$–$10^8$ times. Quantitative analysis of the colony forming units (CFU) of *S. aureus* (c) and *S. mutans* (d). SEM images of *S. aureus* (e) and *S. mutans* (f) after incubating with PU-BL and PU-LE5 for 24 h. *$P < 0.05$, **$P < 0.01$, and ***$P < 0.001$.

This journal is © The Royal Society of Chemistry 2022

*J. Mater. Chem. B*, 2022, **10**, 2602–2616 | **2611**

morphology of the bacteria on the contacting surface of PU-BL and PU-LE5 (Fig. 6e and f). Vividly, the bacteria on the surface of the PU-BL membrane without EG12 could exist in large numbers and maintain a healthy and complete morphosis, while there were almost no living bacteria on the surface of the PU-LE5 membrane, leaving only dead bacteria fragments. The result of the blank control is shown in Fig. S5 (ESI†); the number of colonies could not be counted because there were too many colonies. Besides, we also evaluated the antibacterial properties of the polyurethane membranes to *E. coli* (the typical Gram-negative bacteria, ESI†). It was found that the PU-LE series of polyurethane membranes have a relatively poor antibacterial effect on *E. coli*, which may be due to its relatively complex cell wall consisting of not only a peptidoglycan structure but also an outer membrane. This complex structure can prevent antibacterial agents from penetrating the cell wall and play a barrier role to the bacteria.[60]

In general, the series of PU-LE membranes showed good antibacterial properties on oral pathogenic bacteria, both *S. aureus* and *S. mutans*, which may help the periodontal membrane resist the threat of bacterial infection in the process of periodontal repair.

### 3.4. Mineralization and antioxidant capacity

As reported in the literature, the mussel-inspired catechol structure of LDA can accelerate the deposition of calcium and phosphorus elements in the medium to form hydroxyapatite (HAP) under physiological conditions.[3] This function is called mineralization and has proven to be an effective method for bone regeneration *in vivo*.[61,62] To verify the mineralizing ability, the surface of the polyurethane membranes after immersing in simulated body fluids for 7 days was observed using SEM. As shown in Fig. 7a, a large number of uniform and continuous round minerals were formed on the surface of the polyurethane membranes with LDA, and this is similar to the morphology of HAP that has been reported to be deposited on the surface of mineralized materials.[3,44,62] Then EDX was used to analyze the elemental composition of the circular minerals (Fig. S7, ESI†), and the Ca/P ratio of the circular minerals was very close to that of HAP (1.67). Therefore, the main component of the circular minerals on the surface of polyurethane membranes is HAP, which may help to regenerate the periodontal bone tissue defect. In contrast, there is almost no mineral deposition on the surface of PU-BDO because of the absence of a catechol structure. Meanwhile, the chain extender EG12 and surface morphology also contribute certain effects on mineralization (Fig. 7b). With the increase of the amount of EG12, the diameter of round minerals increases, and the diameter of round minerals on the rough side will be significantly larger than that on the smooth side. This may be contributed by the electrostatic interaction between positively charged quaternary ammonium salts and negatively charged hydroxyapatite.[63] At the same time, a rough surface is more conducive to mineral deposition. It should be noted that the PU-BE sample was not analyzed because it became sticky and could not maintain the membrane structure after 7 days of immersion in simulated body fluids (Fig. S8, ESI†).
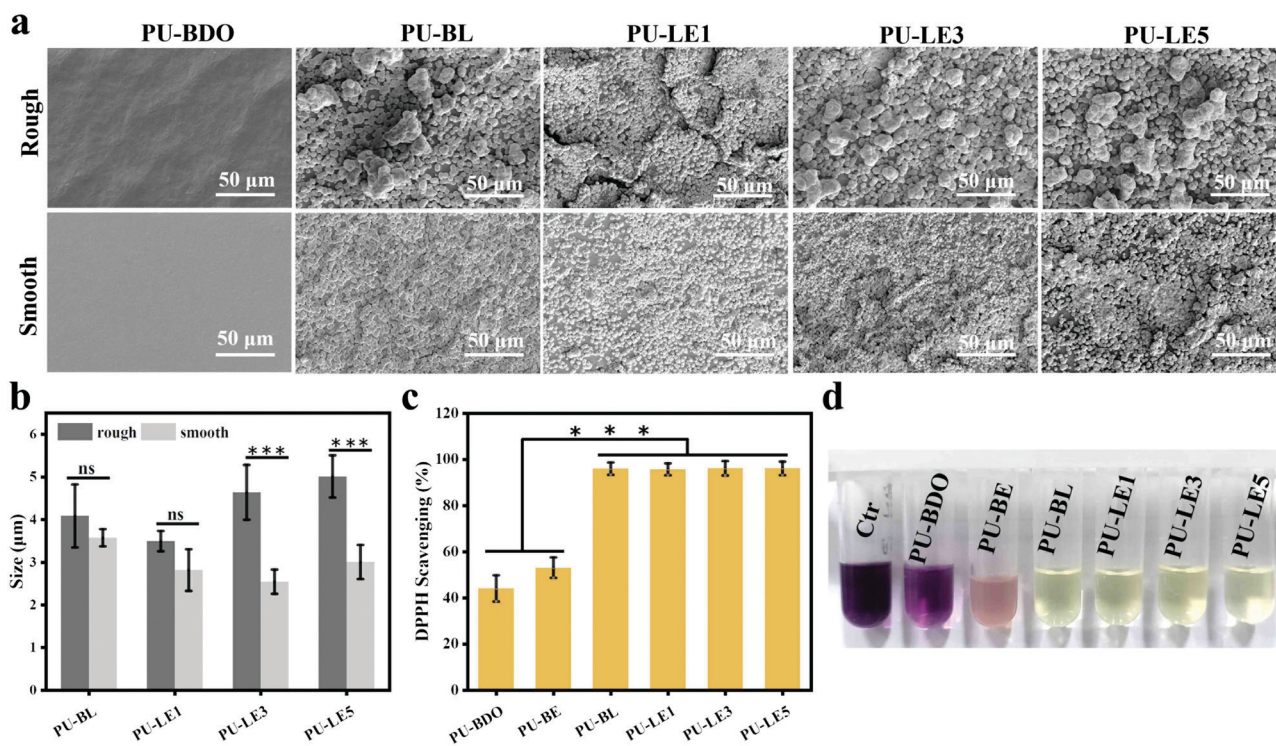


Fig. 7 (a) Mineralization of polyurethane membranes after 7 days immersion in simulated body fluids. (b) The diameter of a round mineral on smooth and rough surfaces. (c) The antioxidant capability of polyurethane membranes. (d) Color change of DPPH after making contact with polyurethane membranes. ***$P < 0.001$.

2612 | *J. Mater. Chem. B*, 2022, **10**, 2602–2616

This journal is © The Royal Society of Chemistry 2022

Excessive accumulation of reactive oxygen species (ROS) in periodontitis sites will damage the body's antioxidant mechanism and cause adverse effects on periodontal cells.[29] Therefore, effective local ROS removal can change the periodontal microenvironment and promote the process of periodontal tissue repair. Herein, the antioxidant capability of polyurethane membranes was quantitatively assessed *via* the ·DPPH-clearance tests. As shown in Fig. 7c, polyurethane membranes containing a chain extender LDA have excellent antioxidant capacity (removal capacity up to 96%). The main reason is that LDA contains a catechol structure. In ethanol solution, ·DPPH and phenol can form a strong hydrogen bond, and electrons are transferred from phenol to •DPPH to realize •DPPH clearance.[43] However, the PU-BDO and PU-BE membranes without LDA also have a partial free radical scavenging ability, which may be related to the easy departure of hydrogen atoms on α-C adjacent to the ether bond of polyurethane in soft segments.[64] The color change to reflect DPPH content is intuitively revealed in Fig. 7d. DPPH is purple at first and turns yellow after the free radical is removed. These results indicate that the series of polyurethane membranes containing LDA have excellent mineralization and antioxidant capacity, which may promote the regeneration of periodontal tissue.

### 3.5. *In vitro* biocompatibility

Since the polyurethane membrane has the potential to be used as an implant material for periodontal tissue regeneration, its biocompatibility is one of the most critical issues to be solved before clinical application. Herein, mouse fibroblasts (L929) and rat bone marrow mesenchymal stem cells (rBMSCs) were chosen to investigate the cytotoxicity of polyurethane membranes *in vitro*. Fig. 8a and b show the cell viability of two kinds of cells co-cultured with the extract of polyurethane membrane for 1 day. The results showed that the cells on all the polyurethane membranes had more than an 80% survival ability at different dilution ratios, showing good biocompatibility and no cytotoxicity.

Gingival epithelial cells and fibroblasts exist in the periodontal tissue. Due to their rapid growth and migration, they can quickly occupy the defective parts of the periodontal hard tissue, resulting in soft tissue covering the defective parts and causing root absorption, which is not beneficial to the regeneration of the periodontal tissue.[8] Therefore, it is expected that the membrane used for periodontal tissue regeneration can exhibit asymmetric function of two sides. One side can assist the reconstruction of bone tissue in the periodontal defect and the other sides can prevent the migration of epithelium and fibroblasts to the defect. In this work, the series of PU-LE membranes constructed with Janus surface morphology have the potential to regulate the cell adhesion on both sides. Fig. 8c and d are the quantitative analysis of adhesion quantity and the live/dead staining images of rBMSCs implanted on rough and smooth surfaces of polyurethane membranes for 3 days. From the analysis of smooth surface alone, the introduction of chain extender LDA in PU-BL membranes can significantly improve
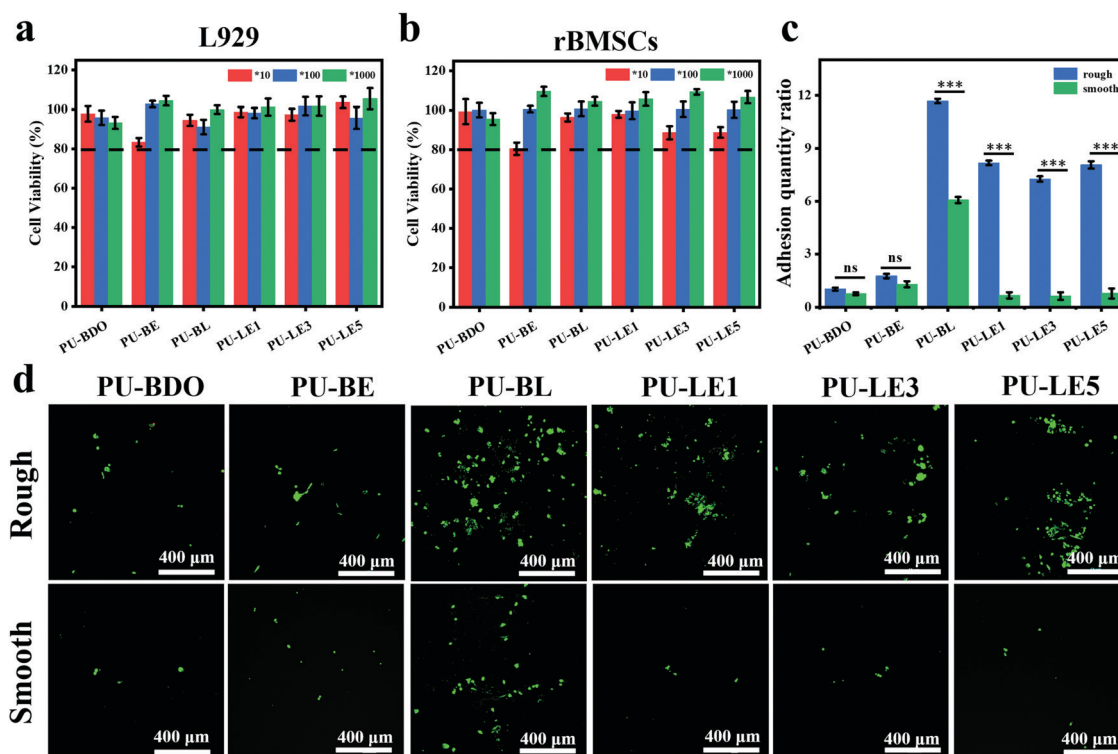


Fig. 8 (a) Cell viability of L929. (b) Cell viability of rBMSCs. 10, 100 and 1000 represent the diluted multiples of the extract of polyurethane membranes. (c) Quantitative analysis of cell adhesion quantity. The adhesion amount of the rough surface of PU–BDO in Fig. 8d was defined as 1. (d) Live/dead staining images of rBMSCs implanted on rough and smooth surfaces of polyurethane membranes for 3 days. Green fluorescence and red fluorescence represent living and dead cells, respectively. ***$P < 0.001$.

This journal is © The Royal Society of Chemistry 2022

*J. Mater. Chem. B*, 2022, **10**, 2602–2616 | **2613**

the cell adhesion ability. This is consistent with the literature report that surface modification with dopamine can improve the cell adhesion of the materials.[3,34] However, when the EG12 was imported in the series of PU-LE membranes, the cell adhesion ability was reduced to a relatively low level. This is because the quaternary ammonium salt will migrate to the surface of polyurethane, resulting in a decrease in the amount of dopamine on the surface.[24] Such cell adhesion behavior corresponds with the results of water contact angle and XPS. Intriguingly, for the rough surface, the series of PU-LE membranes can significantly improve the cell adhesion ability when constructed with special micro-pit morphology. Similar behavior is also shown on the rough surface of PU-BL membranes. There are two possible reasons for this phenomenon. One is the adhesion area increased with such microtopography, and the other is this micro-pit pattern may be more conducive to cell attachment.[8,31,32] Comparatively, the PU-BDO and PU-BE membranes do not show this property because of the absence of the Janus two-sided microstructure and functional groups. In addition to the rBMSCs, the cell behavior of L929 cells on the membranes was also tested (Fig. S9, ESI†), which showed a similar trend as rBMSCs. These results indicate that the series of PU-LE membranes have good biocompatibility and different adhesion ability on the Janus sides. Since the rough surface of the PU-LE membranes with micro-pit morphology can promote the adhesion of rBMSCs as well as excellent capability of autonomic mineralization, this surface of the membrane can be preferably used to face the bone to accelerate bone tissue reconstruction. Meanwhile, the smooth surface of the membrane can be superiorly used to face the soft tissues because of the low cell adhesion to suppress the migration of fibroblasts. Combined with the excellent mechanical property, antibacterial property, and antioxidant capacity, the bioinspired Janus polyurethane membranes will greatly contribute to periodontal tissue regeneration.

### 3.6. Evaluation of periodontal regeneration ability *in vivo*

The excellent comprehensive properties of the Janus polyurethane membrane *in vitro* prompted us to further verify its ability to guide periodontal tissue regeneration *in vivo*. Here, PU-BDO and PU-LE5 were chosen as the experimental objects, the untreated defect group was the blank control, and the complete alveolar bone was the normal control. Fig. 9a is a schematic diagram of the periodontal defect and guided periodontal tissue regeneration. The specific process is shown in Fig. 9b. First, a defect was created on the alveolar bone of the rat maxillary first molar, then the defect was covered with a polyurethane membrane and the wound was sutured. Fig. 9c shows the micro-CT images before defect formation and after 4 weeks of treatment with different membranes. The vertical bone loss of the defect sites was determined by measuring the distance between the alveolar bone crest (ABC) and the cementoenamel junction (CEJ) using Image J software. The result (Fig. 9e) shows that compared with the blank control group, the distance between ABC and CEJ in the PU-BDO group and PU-LE5 group was significantly reduced, and the distance between ABC and CEJ in the PU-LE5 group was smaller, which was close to the normal group. Fig. 9d is the image after three-dimensional reconstruction. It can be seen that the defect site of the blank control group was still obvious, while the PU-BDO group has a section of new bone formation and the defect site was reduced. The PU-LE5 group had the smallest bone defect, showing a good bone recovery effect. The above results show
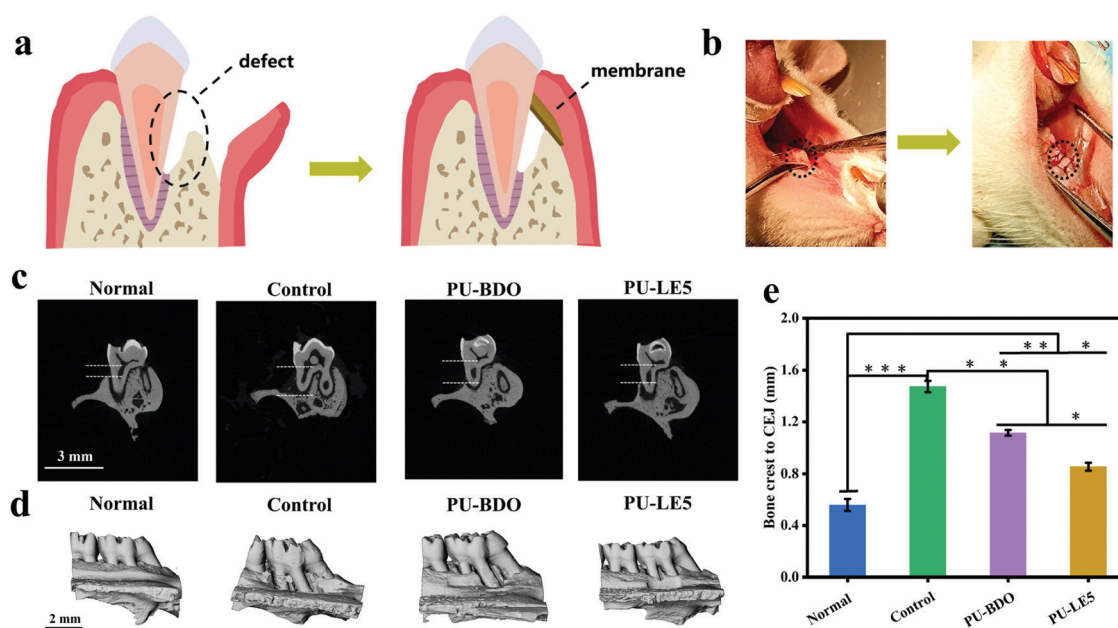


**Fig. 9** (a) Schematic diagram of a rat periodontal defect and guided periodontal tissue regeneration. (b) Digital photographs of periodontal defects and sutured wounds. Sectioned images (c) and three-dimensional reconstructed images (d) of periodontal defects analyzed by micro-CT. (e) The distance between the alveolar bone crest (ABC) and the cementoenamel junction (CEJ) using Image J software. *$P < 0.05$, **$P < 0.01$, and ***$P < 0.001$.

**2614** | *J. Mater. Chem. B*, 2022, **10**, 2602–2616

This journal is © The Royal Society of Chemistry 2022

that this Janus polyurethane membrane has a promoting effect on guiding the regeneration of periodontal tissue.

## 4. Conclusion

In summary, the antibacterial Gemini quaternary ammonium salt and the bioactive dopamine were introduced into polyurethane to develop a series of degradable periodontal membranes with bioinspired Janus morphology. The smooth surface of the membrane can reduce cell adhesion, and the rough surface with a topological micro-pit structure can promote cell adhesion and has excellent mineralization function. *In vitro* research shows that the Janus polyurethanes have excellent mechanical properties, antibacterial properties, antioxidant properties and good biocompatibility. In addition, *in vivo* research also proves that the Janus polyurethane membrane can effectively promote periodontal tissue regeneration in a rat periodontal defect model. Therefore, these bioinspired Janus membranes will have great potential in guiding periodontal tissue regeneration.

## Conflicts of interest

The authors declare no conflict of interest.

## Acknowledgements

## References

1 A. Nasajpour, S. Ansari, C. Rinoldi, A. S. Rad, T. Aghaloo, S. R. Shin, Y. K. Mishra, R. Adelung, W. Swieszkowski, N. Annabi, A. Khademhosseini, A. Moshaverinia and A. Tamayol, *Adv. Funct. Mater.*, 2018, **28**, 1703437.

2 X. Liu, X. He, D. Jin, S. Wu, H. Wang, M. Yin, A. Aldalbahi, M. El-Newehy, X. Mo and J. Wu, *Acta Biomater.*, 2020, **108**, 207–222.

3 M. M. Hasani-Sadrabadi, P. Sarrion, N. Nakatsuka, T. D. Young, N. Taghdiri, S. Ansari, T. Aghaloo, S. Li, A. Khademhosseini, P. S. Weiss and A. Moshaverinia, *ACS Nano*, 2019, **13**, 3830–3838.

4 Y. Zhou, C. Wu and Y. Xiao, *J. Mater. Chem. B*, 2014, **2**, 3907–3910.

5 M. Sanz, A. Marco Del Castillo, S. Jepsen, J. R. Gonzalez-Juanatey, F. D'Aiuto, P. Bouchard, I. Chapple, T. Dietrich, I. Gotsman, F. Graziani, D. Herrera, B. Loos, P. Madianos, J. B. Michel, P. Perel, B. Pieske, L. Shapira, M. Shechter,

M. Tonetti, C. Vlachopoulos and G. Wimmer, *J. Clin. Periodontol.*, 2020, **47**, 268–288.

6 Y. Xu, S. Zhao, Z. Weng, W. Zhang, X. Wan, T. Cui, J. Ye, L. Liao and X. Wang, *ACS Appl. Mater. Interfaces*, 2020, **12**, 54497–54506.

7 X. Niu, L. Wang, M. Xu, M. Qin, L. Zhao, Y. Wei, Y. Hu, X. Lian, Z. Liang, S. Chen, W. Chen and D. Huang, *Carbohydr. Polym.*, 2021, **260**, 117769.

8 F. M. Chen, J. Zhang, M. Zhang, Y. An, F. Chen and Z. F. Wu, *Biomaterials*, 2010, **31**, 7892–7927.

9 D. Abdelaziz, A. Hefnawy, E. Al-Wakeel, A. El-Fallal and I. M. El-Sherbiny, *J. Adv. Res.*, 2021, **28**, 51–62.

10 Y. D. Rakhmatia, Y. Ayukawa, A. Furuhashi and K. Koyano, *J. Prosthodont. Res.*, 2013, **57**, 3–14.

11 Z. Sheikh, J. Qureshi, A. M. Alshahrani, H. Nassar, Y. Ikeda, M. Glogauer and B. Ganss, *Odontology*, 2017, **105**, 1–12.

12 T. Zhou, S. Chen, X. Ding, Z. Hu, L. Cen and X. Zhang, *Front Bioeng. Biotech.*, 2021, **9**, 630977.

13 P. Robert, J. Mauduit, R. M. Frank and M. Vert, *Biomaterials*, 1993, **14**, 353–358.

14 M. C. Bottino, V. Thomas, G. Schmidt, Y. K. Vohra, T.-M. G. Chu, M. J. Kowolik and G. M. Janowski, *Dent. Mater.*, 2012, **28**, 703–721.

15 Y. Liang, X. Luan and X. Liu, *Bioact. Mater*, 2020, **5**, 297–308.

16 Y. Kudo, H. Tada, N. Fujiwara, Y. Tada, T. Tsunematsu, Y. Miyake and N. Ishimaru, *Genes Environ.*, 2016, **38**, 13.

17 N. Li, L. Jiang, H. Jin, Y. Wu, Y. Liu, W. Huang, L. Wei, Q. Zhou, F. Chen, Y. Gao, B. Zhu and X. Zhang, *Colloids Surf., B*, 2019, **183**, 110454.

18 Y. Jiang, Y. Deng, Y. Tu, B. Ay, X. Sun, Y. Li, X. Wang, X. Chen and L. Zhang, *J. Mater. Chem. B*, 2019, **7**, 2634–2642.

19 Z. He, X. Zhou, Y. Wang, J. Lin, S. Huang, R. Hu, Y. Zhou, Q. Qian and H. Deng, *Carbohydr. Polym.*, 2021, **273**, 118525.

20 B. Gu, Z. Liu, K. Zhang, Y. Ji, Y. Zhou and C. Gao, *J. Membr. Sci.*, 2021, **625**, 119112.

21 Z. Geng, Z. Li, Z. Cui, J. Wang, X. Yang and C. Liu, *Nano Lett.*, 2020, **20**, 7716–7721.

22 Y. Yang, T. Xu, H. P. Bei, Y. Zhao and X. Zhao, *Adv. Funct. Mater.*, 2021, **31**, 2104636.

23 B. Du, H. Yin, Y. Chen, W. Lin, Y. Wang, D. Zhao, G. Wang, X. He, J. Li, Z. Li, F. Luo, H. Tan and Q. Fu, *J. Mater. Chem. B*, 2020, **8**, 4434–4446.

24 W. He, Y. Zhang, J. Li, Y. Gao, F. Luo, H. Tan, K. Wang and Q. Fu, *Sci. Rep.*, 2016, **6**, 32140.

25 F. Zhang, R. Wang, Y. He, W. Lin, Y. Li, Y. Shao, J. Li, M. Ding, F. Luo, H. Tan and Q. Fu, *J. Mater. Chem. B*, 2018, **6**, 4326–4337.

26 K. Xiao, Z. Wang, Y. Wu, W. Lin, Y. He, J. Zhan, F. Luo, Z. Li, J. Li, H. Tan and Q. Fu, *J. Biomed. Mater. Res. A*, 2019, **107**, 2205–2221.

27 X. Chen, C. Cortez-Jugo, G. H. Choi, M. Björnmalm, Y. Dai, P. J. Yoo and F. Caruso, *Bioconjugate Chem.*, 2017, **28**, 75–80.

28 L. Ge, Q. Li, Y. Huang, S. Yang, J. Ouyang, S. Bu, W. Zhong, Z. Liu and M. M. Q. Xing, *J. Mater. Chem. B*, 2014, **2**, 6917–6923.

29 X. Bao, J. Zhao, J. Sun, M. Hu and X. Yang, *ACS Nano*, 2018, **12**, 8882–8892.

This journal is © The Royal Society of Chemistry 2022

*J. Mater. Chem. B*, 2022, **10**, 2602–2616 | **2615**

30  G. Murari, N. Bock, H. Zhou, L. Yang, T. Liew, K. Fox and P. A. Tran, *Sci. Rep.*, 2020, **10**, 14982.

31  A. T. Nguyen, S. R. Sathe and E. K. Yim, *J. Phys.: Condens. Matter*, 2016, **28**, 183001.

32  C. Tu and C. Gao, *Chinese J. Polym. Sci.*, 2021, **39**, 815–823.

33  Y. Li, Y. Xiao and C. Liu, *Chem. Rev.*, 2017, **117**, 4376–4421.

34  X. Chen, C. Cortez-Jugo, G. H. Choi, M. Bjornmalm, Y. Dai, P. J. Yoo and F. Caruso, *Bioconjugate Chem.*, 2017, **28**, 75–80.

35  J. Xue, M. He, Y. Liang, A. Crawford, P. Coates, D. Chen, R. Shi and L. Zhang, *J. Mater. Chem. B*, 2014, **2**, 6867–6877.

36  T. Wu, L. Huang, J. Sun, J. Sun, Q. Yan, B. Duan, L. Zhang and B. Shi, *Carbohydr. Polym.*, 2021, **269**, 118276.

37  S. Q. Liu, C. Yang, Y. Huang, X. Ding, Y. Li, W. M. Fan, J. L. Hedrick and Y. Y. Yang, *Adv. Mater.*, 2012, **24**, 6484–6489.

38  S. Li, S. Dong, W. Xu, S. Tu, L. Yan, C. Zhao, J. Ding and X. Chen, *Adv. Sci.*, 2018, **5**, 1700527.

39  Y. Zhang, W. He, J. Li, K. Wang, J. Li, H. Tan and Q. Fu, *Mater. Chem. Front.*, 2017, **1**, 361–368.

40  Y. He, X. Wan, K. Xiao, W. Lin, J. Li, Z. Li, F. Luo, H. Tan, J. Li and Q. Fu, *Biomater. Sci.*, 2019, **7**, 5369–5382.

41  M. He, H. Xiao, Y. Zhou and P. Lu, *J. Mater. Chem. B*, 2015, **3**, 3704–3713.

42  X. Zhao, H. Ming, Y. Wang, F. Luo, Z. Li, J. Li, H. Tan and Q. Fu, *ACS Appl. Bio Mater.*, 2021, **4**, 5352–5361.

43  Y. Feng, K. Xiao, Y. He, B. Du, J. Hong, H. Yin, D. Lu, F. Luo, Z. Li, J. Li, H. Tan and Q. Fu, *Mater. Sci. Eng., C: Mater. Biol. Appl.*, 2021, **121**, 111820.

44  X. Zheng, X. Ke, P. Yu, D. Wang, S. Pan, J. Yang, C. Ding, S. Xiao, J. Luo and J. Li, *J. Mater. Chem. B*, 2020, **8**, 10407–10415.

45  Y. Zhang, Y. Li, J. Li, Y. Gao, H. Tan, K. Wang, J. Li and Q. Fu, *Sci. Bull.*, 2015, **60**, 1114–1121.

46  C. Z. Chen, N. C. Beck-Tan, P. Dhurjati, T. K. van Dyk, R. A. LaRossa and S. L. Cooper, *Biomacromolecules*, 2000, **1**, 473–480.

47  J. H. Wynne, P. A. Fulmer, D. M. McCluskey, N. M. Mackey and J. P. Buchanan, *ACS Appl. Mater. Interfaces*, 2011, **3**, 2005–2011.

48  N. A. Peppas, P. Bures, W. Leobandung and H. Ichikawa, *Eur. J. Pharm. Biopharm.*, 2000, **50**, 27–46.

49  A. A. Putnam and J. J. Wilker, *Soft Matter*, 2021, **17**, 1999–2009.

50  Y. Li and Y. Cao, *Nanoscale Adv.*, 2019, **1**, 4246–4257.

51  L. Tang, X. Long, X. He, M. Ding, D. Zhao, F. Luo, J. Li, Z. Li, H. Tan and H. Zhang, *J. Mater. Chem. B*, 2021, **9**, 3210–3223.

52  Y. Gao, J. Lv, L. Liu and Y. Yu, *e-Polymers*, 2020, **20**, 469–481.

53  M. Nosonovsky, *Langmuir*, 2007, **23**, 9919–9920.

54  X. Ji, Y. Wang, J. Xu and Y. Huang, *Mater. Lett.*, 2017, **195**, 71–75.

55  J. Carnio, J. T. Ribas, D. Lipton and J. Brown, *Clin. Adv. Periodont.*, 2016, **6**, 9–16.

56  R. Serodio, S. L. Schickert, A. R. Costa-Pinto, J. R. Dias, P. L. Granja, F. Yang and A. L. Oliveira, *Mater. Sci. Eng., C: Mater. Biol. Appl.*, 2019, **98**, 969–981.

57  S. B. Qasim, R. M. Delaine-Smith, T. Fey, A. Rawlinson and I. U. Rehman, *Acta Biomater.*, 2015, **23**, 317–328.

58  E. C. Carlo Reis, A. P. Borges, M. V. Araujo, V. C. Mendes, L. Guan and J. E. Davies, *Biomaterials*, 2011, **32**, 9244–9253.

59  C. Li, D. Lu, J. Deng, X. Zhang and P. Yang, *Adv. Mater.*, 2019, **31**, 1903973.

60  S. Lenka, D. Singh, S. Paul, A. Gayen and M. Chandra, *ACS Infect. Dis.*, 2021, **7**, 733–745.

61  S. Bi, P. Wang, S. Hu, S. Li, J. Pang, Z. Zhou, G. Sun, L. Huang, X. Cheng, S. Xing and X. Chen, *Carbohydr. Polym.*, 2019, **224**, 115176.

62  X. Zhang, Y. He, P. Huang, G. Jiang, M. Zhang, F. Yu, W. Zhang, G. Fu, Y. Wang, W. Li and H. Zeng, *Composites, Part B*, 2020, **197**, 108183.

63  Z. He, S. Sun and C. Deng, *J. Bionic Eng.*, 2020, **17**, 345–356.

64  J. R. Martin, P. Patil, F. Yu, M. K. Gupta and C. L. Duvall, *Biomaterials*, 2020, **263**, 120377.

**2616** | *J. Mater. Chem. B*, 2022, **10**, 2602–2616

This journal is © The Royal Society of Chemistry 2022